2D Fokker-Planck Simulations of Short-Pulse Laser-Plasma Interactions

G. J. Rickard and A. R. Bell
Blackett Laboratory, Imperial College of Science and Technology, Prince Consort Road, London SW7 2BZ, United Kingdom

E. M. Epperlein
Laboratory for Laser Energetics, University of Rochester, 250 East River Road, Rochester, New York 14623-1299
(Received 13 December 1988)

The Fokker-Planck equation for electrons in two spatial dimensions in the diffusive approximation is solved by the alternating-direction-implicit method. The ions are modeled hydrodynamically. We discuss simulations of short-pulse (3.5 ps) experiments at a wavelength of $\frac{1}{4}$ μm. We find substantial departures from Spitzer heat flow in both magnitude *and* direction. As a result we find that, even for 10-μm-diam laser spots, the heat flow into the target is not strongly reduced by energy escaping along the target surface.

PACS numbers: 52.50.Jm, 52.25.Fi, 52.65.+z

Fluid codes are widely used in the analysis of laser-plasma experiments.[1] However, to obtain heat flow consistent with experimental data, fluid codes need to limit the heat flow to a fraction f of the local free-streaming heat flow $q_{fs}=n_e k T_e (kT_e/m_e)^{1/2}$, f being the so-called "flux limiter."[2] The problem of evaluating the heat flow in fluid codes in 2D is further complicated, as explained by Strauss *et al.*[3] Now, not only is the magnitude of each component of the heat flow a concern, but also the actual direction of the resultant heat flow $\mathbf{q}$ relative to the local $-\nabla T_e$. As pointed out, this may be especially true in cases where a sufficiently long electron mean free path means that locally defined variables will not adequately describe the heat flow, and there is therefore no reason to suppose that $\mathbf{q}$ and $-\nabla T_e$ will be parallel.

On the other hand Fokker-Planck (FP) codes can self-consistently model non-Spitzer behavior without recourse to flux limiters in both 1D,[4] and, more recently 2D,[5] and it is the 2D code that forms the basis of this paper. The details of the 2D code have been given elsewhere.[6] There we show that alternating-direction-implicit (ADI) differencing of the FP equation has enabled fast and reliable kinetic simulations to be performed. The code was previously used to examine nonlocal smoothing in laser-produced plasmas.[5] Here the code is used to examine the conditions applicable to recent experiments by Willi *et al.*[7] in which hot ($T_e \approx 400$ eV), high-density ($n_e \geq 10^{23}$ cm^{-3}) plasmas have been produced by picosecond laser pulses without a prepulse. Such plasma parameters are important for basic plasma and atomic physics studies as well as for x-ray laser research.[8] As we show later, the concern voiced by Strauss *et al.* about the nature of the 2D heat flow is to some extent borne out by our results from the simulations of these short-pulse experiments.

We model the interaction of a $\frac{1}{4}$-μm laser of peak intensity 6×10^{15} W cm^{-2} and FWHM = 3.5 ps with a fully ionized aluminum target ($Z=13$) with an initial density profile at $t=0$ ps assumed as shown in Fig. 1(a), and with an initial uniform temperature of 100 eV. Laser energy deposition is modeled with the inverse bremsstrahlung (IB) operator as given by Langdon.[9] Other absorption processes may also be operative,[7] but IB is sufficient to give 30% energy absorption at peak laser intensity. The exponential ramp joining the upper and lower density plateaus has a scale length of 3 μm, and the initial maximum density is 8×10^{22} cm^{-3}, parameters more severe than those modeled previously[10,11] where scale lengths of 50–100 μm and densities of 2×10^{22} cm^{-3} are typically used. The z direction is into

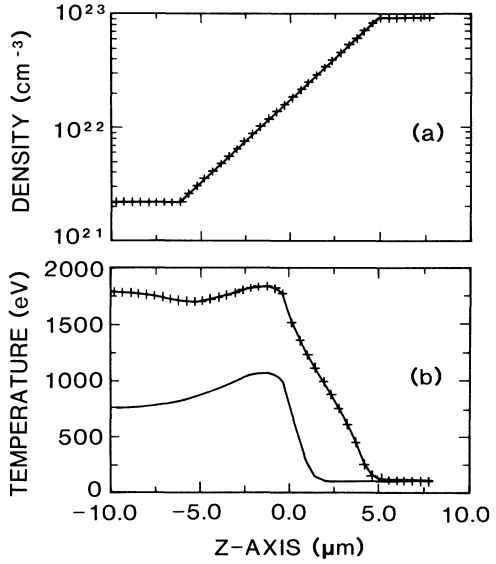

FIG. 1. (a) Initial electron density profile. (b) Temperature profiles from the 1D FP code at 3 ps (continuous line) and 6 ps (line with crosses).

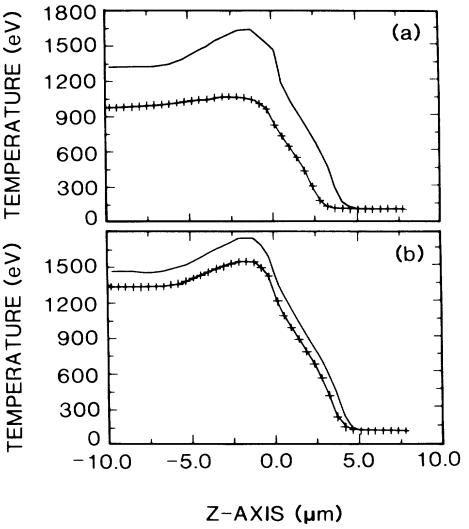

FIG. 2. Temperature profiles at $x=0$ μm (continuous line) and $x=9$ μm (line with crosses) for (a) 10-μm and (b) 20-μm spot sizes from the 2D FP code at 6 ps.

the target, and the x direction is across the target. The target extends from $x=0$ to 40 μm. Spatially Gaussian profiles for the laser intensity in x are assumed, centered at $x=0$ μm, with FWHM of 10 and 20 μm. Twenty spatial cells are used in x, forty in z, and forty uniformly spaced velocity cells. For comparison, the simulations were also performed with a standard 2D fluid code using uninhibited Spitzer-Harm heat flow $\mathbf{q}_{\mathrm{Sp}}=-K\nabla T_e$,[12] and a 1D version of the 2D FP code.

The penetration of the heat front into the solid is shown in Fig. 1(b), which gives the profiles of the temperature at 3 and 6 ps from the 1D code. The irradiances on the axis $x=0$ μm from the 2D FP code are used in the 1D code. Figures 2(a) and 2(b) show the temperature profiles from the 2D FP code at 6 ps for the 10- and 20-μm laser intensity spot sizes, respectively. In Figs. 2(a) and 2(b) the continuous line is data on the axis $x=0$ μm, while the lines with crosses are taken 9 μm off axis. Comparing 2(a) and 2(b) we see that the on-axis profiles are within 110 eV of each other. These on-axis profiles are also comparable to the 1D temperature profile at 6 ps in Fig. 1(b). The profiles at 9 μm, however, clearly demonstrate the effect of the spot sizes, the temperature maximum for the 10-μm case being lower at 6 ps by approximately 500 eV than for the 20-μm case. The similarity of the on-axis profiles suggests that the lateral heat flow is not very important in determining the maximum temperature attained over such short time scales. The profiles in 2(a) and 2(b) also show the characteristics of non-Spitzer heat flow, i.e., a sharp drop from the maximum temperature and a small, low-temperature foot to the heat front.

The temperature contours from the 2D FP code at 6 ps for the 10-μm laser spot are shown in Fig. 3(a). This

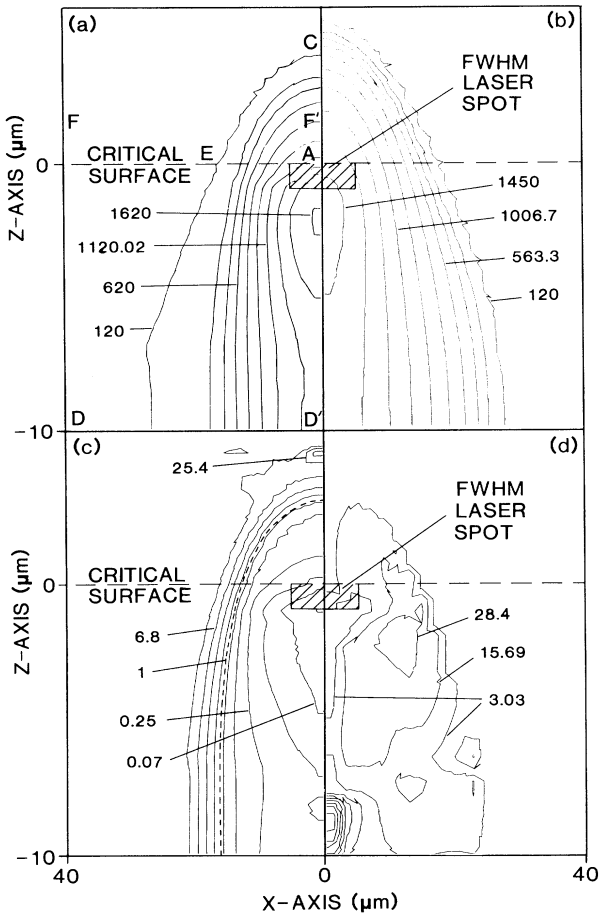

FIG. 3. Contours at 6 ps for the 10-μm spot size of (a) temperature in eV from the 2D FP code (contour interval 166.67 eV), (b) temperature in eV from the 2D Spitzer code (contour interval 147.78 eV), (c) $|\mathbf{q}|/|\mathbf{q}_{\mathrm{Sp}}|$, and (d) the angle θ between $\mathbf{q}$ and $-\nabla T_e$ (see text).

figure reveals a temperature front that lies approximately 4 μm from the critical surface along a line into the target, with the front approximately 28 μm from the axis in the lateral direction in the subcritical plasma. In contrast Fig. 3(b) shows the temperature contours for the same conditions from the 2D Spitzer code. We see that the Spitzer code predicts the position of the temperature front (as represented by the 120-eV contour) to be approximately 1.5 μm further both into and across the target relative to the FP temperature front. Also, by comparing the FP and Spitzer temperature profiles both axially and laterally (not shown), we find that the lower part of the FP temperature front is much shallower than that predicted by the 2D Spitzer code. Indeed, the Spitzer temperature profile is steep at the solid surface (characteristically a $T_e^{5/2}$ temperature scale-length dependence in the region of the temperature front in steady state). This could mean an overestimate of the position of the Spitzer temperature front if there is

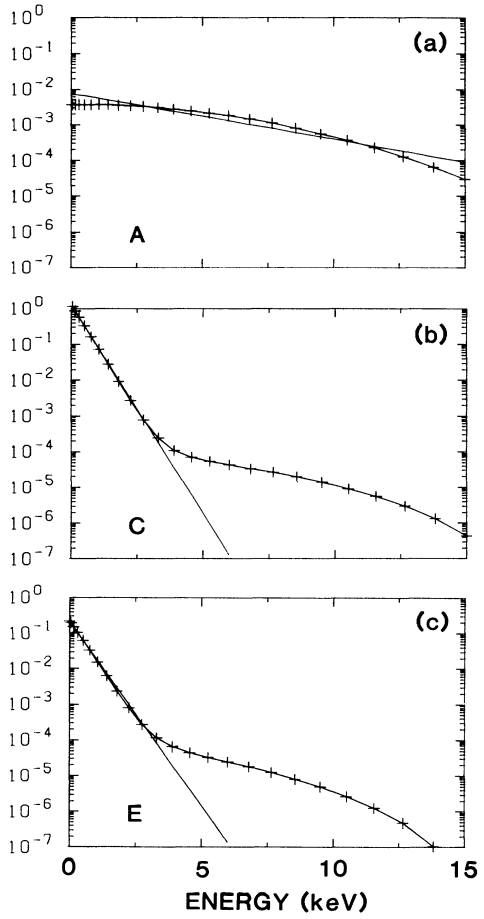

FIG. 4. Electron distribution functions (line with crosses) and local Maxwell-Boltzmann distributions (continuous line) at various positions as labeled in Fig. 3(a).

inadequate numerical resolution, although the 1.5-μm excess of the Spitzer code into the target is resolved by approximately four grid points.

The nonclassical nature of the heat flow is also evident in Fig. 3(c), a contour plot of $|\mathbf{q}|/|\mathbf{q}_{\mathrm{Sp}}|$ at 6 ps, where $\mathbf{q}_{\mathrm{Sp}}$ is the Spitzer heat flow calculated from the temperatures found by the 2D FP code, as contoured in Fig. 3(a). The dotted line in Fig. 3(c) is the approximate position of the contour for $|\mathbf{q}| = |\mathbf{q}_{\mathrm{Sp}}|$. At the top of the heat front in the region of the laser spot we see that $|\mathbf{q}|/|\mathbf{q}_{\mathrm{Sp}}| \leq 1$, while this ratio is greatly enhanced (≥ 13) at the bottom of the heat front. Figure 3(c) also reveals a small "foot" to the FP heat flow where $|\mathbf{q}|/|\mathbf{q}_{\mathrm{Sp}}| = 25.4$, which is not evident in Fig. 3(a). However, close examination of Fig. 2(a) at $z = 5$ μm does indeed show a small but finite low-temperature foot that is characteristic of FP calculations, and which is not resolved by the contours in Fig. 3(a). Furthermore, Fig. 3(d), a contour plot of θ, the difference in angle between the direction of the local FP heat flow and the Spitzer heat flow, i.e.,

$$\theta = \{\tan^{-1}(q_z/q_x) - \tan^{-1}(q_{\mathrm{Sp}z}/q_{\mathrm{Sp}x})\},$$

reveals regions where the heat flow is not parallel to the local temperature gradients, and that θ can be up to 34°. This possibility was previously pointed out in the context of the application of flux limiters in 2D in fluid codes.[3] In the supercritical plasma, and indeed even where $-\nabla T_e$ is lateral, Fig. 3(d) also shows that the heat flow is preferentially directed into the target.

Figures 4(a)–4(c) show $f_0(v)$, the isotropic component of the electron distribution, with the local Maxwell-Boltzmann distribution at the various positions in Fig. 3(a). Distributions such as these have been described in previous 1D FP simulations.[10] At position A plotted in Fig. 4(a) we see the characteristic depletion of the low-velocity electrons due to the action of the laser for densities below critical (the Langdon effect[9]), as well as depletion of high-velocity electrons due to transport. At the bottom of the temperature front at C, Fig. 4(b), we see an enhanced high-velocity tail due to the presence of the long-range, hot electrons escaping from the region around critical. We note that for our 2D FP simulations the isotropic components of the distribution along the line A to E across the target are very similar to those along the line A to C into the target. This can be seen by comparing Figs. 4(b) and 4(c) for positions C and E, respectively, where E has been chosen to lie on approximately the same temperature contour as C.

Figures 5(a)–5(c) are a series of plots from the 2D FP code of $|\mathbf{q}\cdot\mathbf{z}'|/q_{\mathrm{fs}}$ (the crosses) and $|\mathbf{q}_{\mathrm{Sp}}\cdot\mathbf{z}'|/q_{\mathrm{fs}}$ (the lines) against $|L_{z'}|/\lambda$, where $L_{z'} = T_e/(\mathbf{z}'\cdot\nabla T_e)$ is the temperature scale length, λ is the local thermal electron mean free path, and $\mathbf{z}'$ is the unit vector in each direction. Figure 5(a) is for the component into the target along the axis. From this we see that $|q_z|/q_{\mathrm{fs}}$ does not exceed 0.1 for any $|L_z|/\lambda$, that the heat flow can be multivalued for a given $|L_z|/\lambda$, and that $|q_z|/q_{\mathrm{fs}}$ can be much greater than the calculated $|q_{\mathrm{Sp}z}|/q_{\mathrm{fs}}$ for the same $|L_z|/\lambda$. This behavior is repeated for all values of x. A flux limiter of $f = 0.1$, then, would keep the magnitude of the Spitzer heat flow into the target less than or equal to the maximum value attained by the FP heat flow for the same temperature distribution. Such a value of f has been obtained in previous FP calculations.[4] However, a simple flux limitation does not reproduce the FP heat flow for a given $|L_z|/\lambda$. Figure 5(b) shows the lateral component in the supercritical plasma along the line FF′ to be much less than both the heat flow into the target and 0.1 of q_{fs}. However, Fig. 5(c) along the line DD′ shows that the lateral component in the hot, subcritical plasma (a region in which the diffusive approximation should be treated with caution) can be well in excess of 0.1 of q_{fs}, although the total energy carried by this lateral heat flow is relatively small in comparison to the energy carried into the target beyond critical. In this

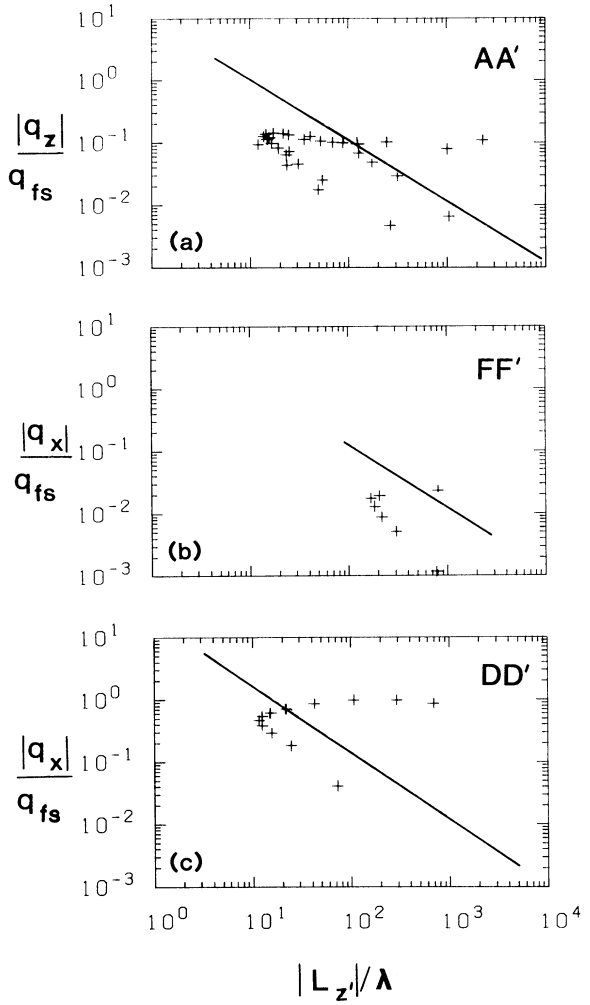

FIG. 5. Plots of $|\mathbf{q}|/q_{fs}$ (the crosses) and $|\mathbf{q}_{Sp}|/q_{fs}$ (the lines) against $|L_{z'}|/\lambda$ (see text). (a) $|q_z|/q_{fs}$ and $|q_{Spz}|/q_{fs}$ along the axis. (b), (c) $|q_x|/q_{fs}$ and $|q_{Spx}|/q_{fs}$ along the lines FF' and DD', respectively, as shown in Fig. 3(a).

particular instance, then, a flux limiter of $f=0.1$ used in the lateral direction would not affect the lateral supercritical heat flow as its value is much less than 0.1 of q_{fs} anyway. However, the heat flow in the subcritical plasma would be reduced by nearly an order of magnitude below that predicted by the FP simulation by such a flux limitation.

In summary, our 2D FP simulations of short-pulse laser-plasma interactions have self-consistently revealed nonclassical heat flow in terms of both magnitude and direction. The heat flow into the target does not exceed 0.1 of q_{fs}, while the lateral heat flow is much less than 0.1 of q_{fs} in the supercritical plasma and of the order of q_{fs} in the hot, low-density corona. Also, the angle between $\mathbf{q}$ and $-\nabla T_e$ can be up to 34°, resulting in a heat flow that is preferentially directed into the target. The outcome, in this case, is 2D simulations that behave in a more one-dimensional fashion than they might otherwise have been expected to. However, simulations with different initial density scale lengths, intensities, etc., are required before we are able to say whether this particular nonclassical behavior is restricted to the severe conditions in these short-pulse experiments, or is a more general feature of 2D heat flow. If the latter is true, then it may eventually be possible to equip 2D fluid codes with parameters equivalent to the flux limiter f in 1D fluid codes, which will reproduce the correct magnitude and direction of the heat flow in terms of the locally defined electron density and temperature.

We are grateful to I. R. G. Williams for his help in running the 1D FP code. This work was supported by the Science and Engineering Research Council, United Kingdom, and by the U.S. Department of Energy Office of Inertial Fusion under Agreement No. DE-FC08-85DP40200 and by the Laser Fusion Feasibility Project at the Laboratory for Laser Energetics which has the following sponsors: Empire State Electric Energy Research Corporation, New York State Energy Research and Development Authority, Ontario Hydro, and the University of Rochester.

[1]M. H. Emery, J. H. Orens, J. H. Gardner, and J. P. Boris, Phys. Rev. Lett. **48**, 253 (1982); R. G. Evans, Laser Part. Beams **3**, 273 (1985); R. D. Jones, W. C. Mead, S. V. Coggeshall, C. H. Aldrich, J. L. Norton, G. D. Pollak, and J. M. Wallace, Phys. Fluids **31**, 1249 (1988).

[2]R. C. Malone, R. L. McCrory, and R. L. Morse, Phys. Rev. Lett. **34**, 721 (1975).

[3]M. Strauss, G. Hazak, D. Shvarts, and R. S. Craxton, Phys. Rev. A **30**, 2627 (1984).

[4]A. R. Bell, R. G. Evans, and D. J. Nicholas, Phys. Rev. Lett. **46**, 243 (1981).

[5]E. M. Epperlein, G. J. Rickard, and A. R. Bell, Phys. Rev. Lett. **61**, 2453 (1988).

[6]E. M. Epperlein, G. J. Rickard, and A. R. Bell, Comput. Phys. Commun. **52**, 7 (1988).

[7]O. Willi *et al.* (to be published).

[8]G. J. Pert, Plasma Phys. Controlled Fusion **27**, 1427 (1985).

[9]A. B. Langdon, Phys. Rev. Lett. **44**, 575 (1980).

[10]J. R. Albritton, Phys. Rev. Lett. **50**, 2078 (1983).

[11]J. P. Matte, T. W. Johnston, J. Delettrez, and R. L. McCrory, Phys. Rev. Lett. **53**, 1461 (1984).

[12]L. Spitzer, Jr., and R. Harm, Phys. Rev. **89**, 977 (1953).